ACS APPLIED ENERGY MATERIALS
Cite This: ACS Appl. Energy Mater. XXXX, XXX, XXX−XXX
Letter
www.acsaem.org

Symmetric All-Quinone Aqueous Battery

Liuchuan Tong,[§,†] Yan Jing,[§,†] Roy G. Gordon,[*,†,‡] and Michael J. Aziz[*,‡]

[†]Department of Chemistry and Chemical Biology, Harvard University, Cambridge, Massachusetts 02138, United States
[‡]John A. Paulson School of Engineering and Applied Sciences, Harvard University, Cambridge, Massachusetts 02138, United States

Supporting Information

ABSTRACT: Here we report a symmetric all-quinone aqueous battery based entirely on earth-abundant elements that uses a naturally occurring dye as the redox-active material in both positive and negative electrodes. We demonstrated a symmetric all-quinone cell with 1.04 V of open circuit voltage, 163 mAh/g of capacity, and 100 cycles at 10C with 100% of depth of discharge. The use of the same quinone in a symmetric setup expands the repertoire of inexpensive redox-active materials for aqueous rechargeable batteries, and the simple cell design will enable optimizations toward safe, cheap, light-weight, and flexible electronics in future.

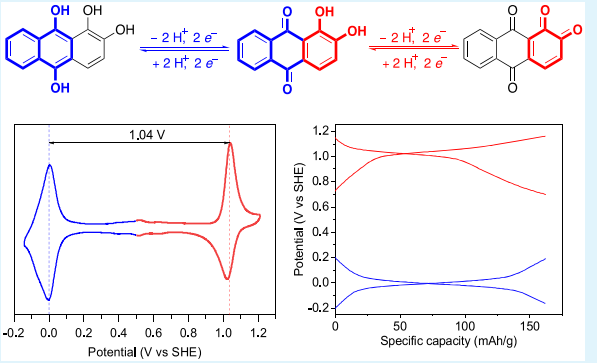

KEYWORDS: *symmetric, metal-free, quinone, three-states, aqueous, proton battery*

Lithium-ion batteries continue to dominate the portable electronic and electric vehicle markets for its high energy density/specific energy.[1] However, combustible electrolytes and expensive cathodes pose safety and cost concerns to consumers.[2] Further cost reduction is expected to be limited after decades of development.[3] Next generation energy storage devices call for safe, cheap, resource-abundant, and flexible batteries.[2,4] Rechargeable batteries with cost-effective redox-active materials and aqueous electrolytes can potentially meet these requirements.[5] Currently, the lead−acid battery (LAB) has the largest market share among aqueous batteries and continues to be attractive for its wide availability and competitive price.[6] However, in addition to the obvious environmental concerns of lead,[7] the LAB has fundamental chemistry challenges during cycling. Sulfuric acid electrolyte participates in the redox chemistry, and sulfation, a build-up of lead sulfate crystals on electrodes over cycling, incurs mechanical stress and penalizes cycle life significantly.[8] Therefore, the LAB can be cycled only with a shallow depth of discharge (DoD), and a trade-off between effective energy density and cycle life is inevitable. Nickel−metal hydride aqueous batteries suffer from similar volume expansion problems, and some use expensive rare-earth metals in the anode.[9] Emerging aqueous rechargeable lithium/sodium-ion batteries utilize electrode materials (particularly the cathodes) similar to those used in nonaqueous lithium/sodium-ion batteries, but they have less than half of the voltage (<1.5 V) of their nonaqueous counterparts,[10] penalizing their economics.

Organic electrode materials, which consist of earth-abundant elements such as C, H, and O and are synthesized at a much lower temperature (<200 °C) than their inorganic counterparts (>500 °C),[4] are becoming promising candidates for the next generation of sustainable energy storage devices.[11] Quinones are a class of organic molecules that are ubiquitous in nature and known to participate in a fast, two-electron redox process via a proton-coupled electron-transfer (PCET) mechanism.[12] Quinones have been explored in the context of nonaqueous solid batteries[13] and aqueous flow batteries.[14] More recently, Liang et al. investigated quinones as anodes in aqueous solid batteries.[15] However, cathodes remained inorganic, e.g., lead dioxide, lithium magnesium oxide/lithium cobalt oxide, nickel oxyhydroxide, etc. We report here the use of a single quinone molecule as both negative and positive electrode material in a symmetric cell. The concept of a symmetric cell system has been proposed in various battery systems for its simplicity in design and has been demonstrated in both nonaqueous flow battery[16] and solid-electrode battery communities.[17,18] The redox-active materials in symmetric cells could be organics,[17] inorganics,[18] or organometallic complexes.[19] In order to build a symmetric cell, the redox-active material must have at least three stable oxidation states. For example, inorganic metal complexes have multiple oxidation states.[18] Organic molecules often delocalize charges in extended π-electron systems such as porphyrins,[20] or have bipolar functional groups,[17] but these functional groups are usually incompatible with aqueous systems.

Motivated by recent success in the development of anthraquinone-based negative electrolyte materials for high-performance aqueous flow batteries,[14,21−23] we explore the

Received: April 3, 2019
Accepted: May 28, 2019

DOI: 10.1021/acsaem.9b00691
ACS Appl. Energy Mater. XXXX, XXX, XXX−XXX

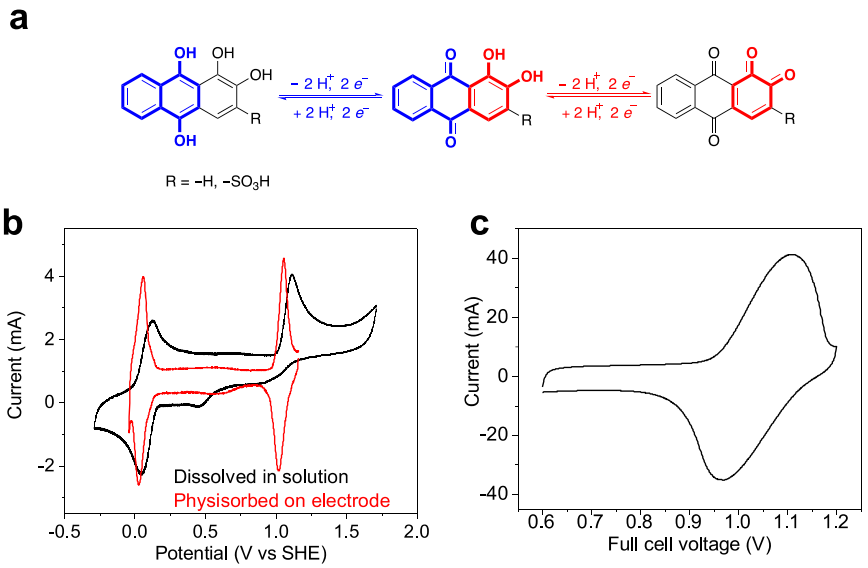

Figure 1. PCET working mechanism and corresponding cyclic voltammetry (CV) curves. (a) Alizarin (center) accepting two electrons and two protons to become fully reduced (left), or donating two electrons and two protons to become fully oxidized (right) in redox reactions. (b) CVs of alizarin sulfonate (R = SO_3^-) dissolved in solution and physisorbed on a carbon paper electrode in 1 M H_2SO_4, scan rate: 10 mV/s. Positive current is oxidative. The scanning range is −0.25 to 1.75 V vs SHE for alizarin sulfonate dissolved in solution, and −0.05 to 1.20 V vs SHE for alizarin sulfonate physisorbed on electrode. (c) Full cell CV curve from the symmetric full cell on flexible carbon cloth.

third oxidation state of a fused anthraquinone, alizarin, in a single-compound battery. Alizarin, historically used as a natural dye, exists in abundance in plants of the madder genus and was the first natural dye to be synthesized at an industrial scale.[24] When two quinone motifs fuse together (Figure 1a), three oxidation states exist in one single anthraquinone molecule. During charging, the center *para*-quinone motif can be reduced into *para*-hydroquinone on the negative side to form fused-hydroquinone, and the right *ortho*-hydroquinone motif can be oxidized into *ortho*-quinone on the positive side to form fused-quinone. Conversely, during discharging, the fused-hydroquinone and fused-quinone would comproportionate back to alizarin electrochemically. Therefore, compared to LABs, these PCET processes in a solid battery may lead to a relatively smaller volume change of redox-active materials and induce less mechanical stress in electrodes as a result of minimal changes in molecular structure.

To investigate the redox activity of the system, a cyclic voltammetry (CV) study of a soluble alizarin, alizarin sulfonate, was undertaken. As expected, the low-potential redox couple showed excellent redox activity near 0 V vs standard hydrogen electrode (SHE); however, no reduction signal was observed for the high-potential redox couple, which exhibited an abnormally high oxidation peak (Figure 1b). Such behavior was not specific to alizarin but was also observed for other fused quinones, including quinizarin and other fused quinone derivatives. In previous work, Carretero-González et al. discovered that a reversible CV at high potential can be obtained on a working electrode with microcavities filled with alizarin and carbon particles,[25] but it was unclear what caused the difference in the observed redox behavior.

To probe whether the oxidation product is unstable, we chemically synthesized the oxidized alizarin in its tetra-one form (fused-quinone) and found it to be stable in aqueous solution (Figures S1 and S2). In alizarin sulfonate, only at high CV scan rates (>5 V/s) did the high-potential reduction peak appear and become more symmetric with its oxidation peak, indicating that the oxidized form appears only to be stabilized in the solid state (as an adsorbate or insoluble solid) (Figures S2 and S3). It was hypothesized that the alizarin undergoes two separate one-electron processes during oxidation, and in solution the intermediate radical may diffuse away and cause subsequent degradation before it is oxidized to the stable tetra-one form (Scheme S1).[26] Therefore, we reasoned that improved electrochemical reversibility at high potential is feasible if the electron-transfer kinetics of the oxidation process can be enhanced by maintaining intimate contact between the molecules and the conducting material. Indeed, when alizarin sulfonate was preadsorbed onto carbon paper (Scheme S2), and used directly as the working electrode, a reversible redox process was observed for the high-potential part of the molecule even at the slow CV scan rate of 10 mV/s (Figure 1b). We attribute the improved kinetics and stability to the ability to rapidly complete the two-electron transfer between the carbon electrode and adsorbed alizarin sulfonate. The adsorbed alizarin sulfonate displayed two sets of reversible and symmetrical redox peaks.

The difference in potentials provides an opportunity to build a 1 V battery within the 1.23 V thermodynamic water stability window. Solubilizing groups, which are usually attached on quinones for solubility improvement in flow batteries, were found to be irrelevant to the observed behavior, and unfunctionalized, insoluble alizarin displayed the same behavior when adsorbed on carbon paper (Figure S4). As a proof-of-concept of symmetric quinone redox couple, a pseudocapacitor was assembled using two sheets of high-surface-area flexible carbon cloth (Spectracarb 2225 Type 900 activated carbon fabric) with adsorbed alizarin on both terminals. The full cell voltage was 1.04 V at 50% SOC (Figure 1c). This flexible symmetric aqueous quinone pseudocapacitor was successfully subjected to 200 consecutive deep charge−discharge cycles (Figure S5).

Encouraged by the performance of the alizarin-based flexible pseudocapacitor, for which the physioadsorbed redox-active

DOI: 10.1021/acsaem.9b00691
ACS Appl. Energy Mater. XXXX, XXX, XXX−XXX

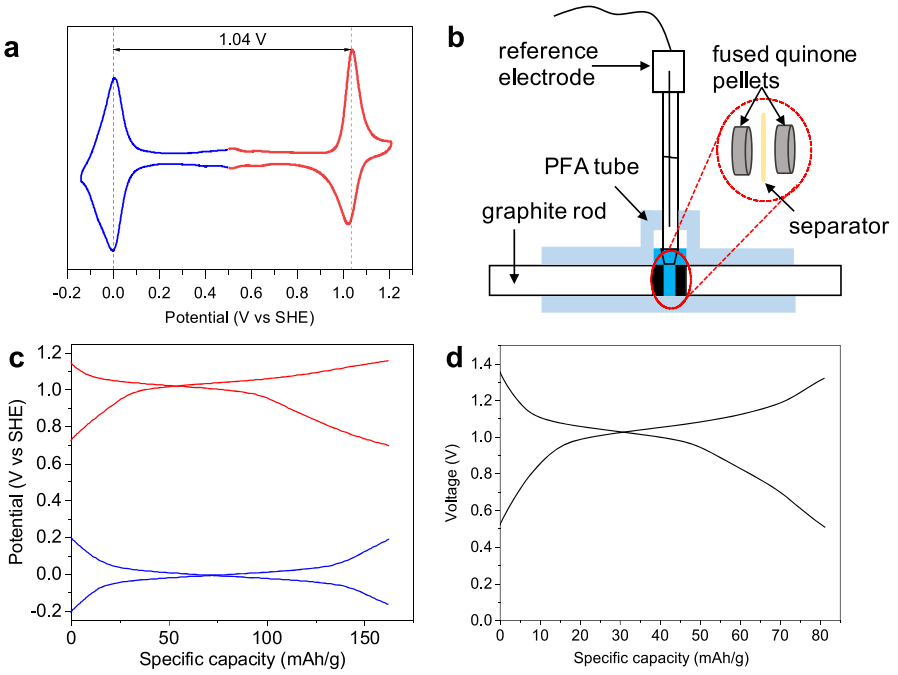

Figure 2. Electrochemical characterization of alizarin-based electrode. (a) The CV curve of ball-milled composite in 1 M H_2SO_4. The ball-milled alizarin/ketjen black/graphite composite (mass ratio: w/w/w = 3:6:1) was first suspended in acetone with a concentration of 10 mg/mL and then drop cast on a glassy carbon working electrode. Scan rate: 100 mV/s. (b) Schematics of alizarin-based three-electrode full cell. (c) Voltage profiles of alizarin as positive (red) and negative (blue) materials, respectively. (d) The full cell voltage (1.0 V) of alizarin-based balanced cell. The specific capacity is based on the total quantity of alizarin active material on both electrodes. The theoretical capacity of alizarin is 223.3 mAh/g.

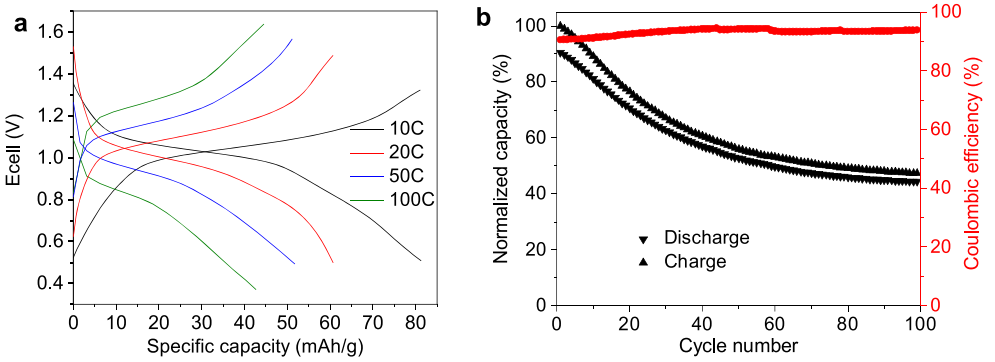

Figure 3. Symmetric alizarin cell performance. (a) The rate performance of the symmetric alizarin cell at 10, 20, 50, and 100C. 1C = 223.3 mA/g. The specific capacity is based on the total quantity of alizarin active material on both electrodes. (b) Cycling stability of the alizarin cell at 10C. The negative electrode is the capacity-limiting side. The positive electrode is the non-capacity-limiting side.

material was limited to only a few monolayers on the carbon surface, we sought to increase the loading of active material to achieve a practically useful energy density. Therefore, commercial alizarin powder was ball-milled with Ketjenblack (Figure S6) to mimic in a battery electrode the intimate contact between redox-active material and electron conducting material apparent in the pseudocapacitor. The mixture exhibited the expected redox activity in CV (Figure 2a). We assembled a three-electrode symmetric cell using nominally identical pellets of the composite as both positive and negative electrode, separated by a hydrophilic porous separator (Celgard coated PP 3401). A Ag/AgCl reference electrode was immersed in the 1 M sulfuric acid electrolyte near the separator (Figure 2b). This setup allowed us to monitor the performance of both electrodes simultaneously and independently. Figure 2c shows the charge−discharge voltage profiles of both electrodes at a C-rate of 10 C (10 mA/cm^2) with a clear voltage plateau of 1 V for high potential and 0 V for low potential; these are in excellent agreement with the CV measurement. The full cell voltage profile of this symmetric cell was plotted in Figure 2d. It shows an average voltage of 1 V and accessed a specific capacity of 81.5 mAh/g, which is based on total quantity of alizarin on both electrodes and is 73.0% of the theoretical value.

The electrochemical performance of the symmetric alizarin cell was further evaluated. Figure 3a showed the specific capacities and voltage profiles at different current rates. When the total quantity of alizarin active material on both electrodes was considered, the discharge capacities were 81.5, 60.5, 51.5, and 42.5 mAh/g, and the midpoint discharge voltages are 1.00, 0.95, 0.87, and 0.74 V when the cell was cycled at 10, 20, 50, and 100C, respectively. The overpotential increases and the capacity decreases with increasing current density. Figure 3b shows the results of cycling of the alizarin-based symmetric full

DOI: 10.1021/acsaem.9b00691
ACS Appl. Energy Mater. XXXX, XXX, XXX−XXX

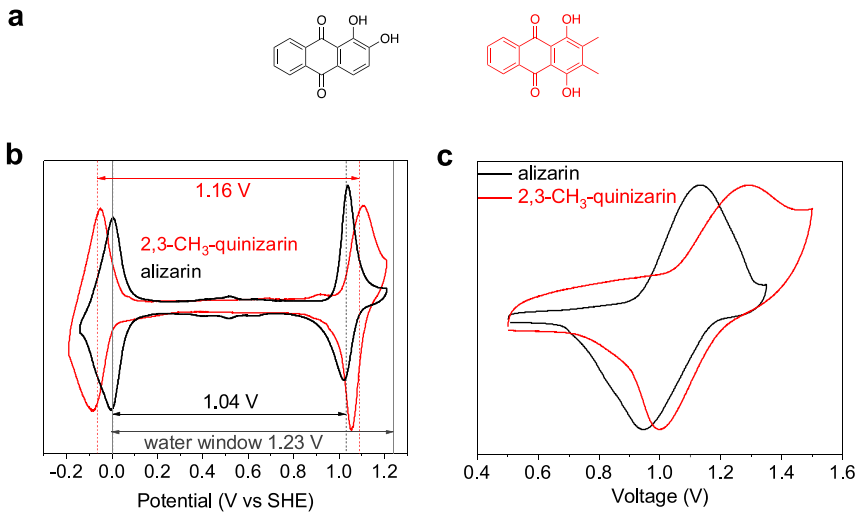

Figure 4. Alternative symmetric quinone. (a) Structures of alizarin and 2,3-dimethyl-quinizarin (2,3-CH_3-quinizarin). (b) CV of 2,3-CH_3-quinizarin compared to alizarin. Scan rate: 100 mV/s. 2,3-CH_3-quinizarin (red) has a broader voltage window compared to alizarin (black). (c) The full cell voltage of 2,3-CH_3-quinizarin symmetric cell compared to alizarin symmetric cell.

cell at 10C; the negative side is capacity-limiting. This unoptimized cell retained 47% of its initial capacity after 100 cycles of full charge and discharge, and the Coulombic efficiency stabilized at 95%.

To gain insight into the capacity loss of the full cell, cycling performance of each terminal was evaluated independently with respect to the reference electrode. We found that the positive terminal capacity decayed at a much higher rate than the anode capacity when cycled at 10C (Figure S7). The ^{1}H NMR spectra of cycled alizarin from the negative terminal remained unchanged, whereas decomposition was observed in alizarin samples from the positive terminal after 200 cycles (Figures S8 and S9). In addition to the possible radical decomposition as discussed above, the highly electron-deficient oxidized alizarin is subject to decomposition via Michael addition, as observed in other high-potential quinones.[27,28]

The use of organic material permits the modification of the molecular structure to fine-tune the desired properties. A preliminary study into the synthesis of other fused quinone derivatives suggests that it is possible to increase the cell voltage and decrease the molecular decomposition rate. For instance, Figure 4a showed the structure of another modified fused quinone, 2,3-dimethyl-quinizarin (2,3-CH_3-quinizarin). The molecule was specifically designed to prevent the attack from Michael addition by nucleophiles on the electrophilic C−H positions on the oxidized fused-quinone form. The methyl group is hypothesized to prevent the nucleophilic decomposition through steric hindrance. To confirm the presumed stability enhancement, we chemically synthesized oxidized 2,3-dimethyl-quinizarin and its unprotected precursor, oxidized quinizarin. The oxidized quinones were stirred with 1 M sulfuric acid overnight and analyzed by ^{1}H NMR (Figures S10 and S11). As expected, hydroxide addition onto the unprotected quinizarin was observed, whereas the protected 2,3-CH_3-quinizarin remained unchanged with only a trace amount of self-discharged 2,3-CH_3-quinizarin due to its highly oxidative nature, confirming the protective nature of the two methyl groups. Upon comparison to alizarin, 2,3-dimethyl-quinizarin has an extended potential window (1.16 V) (Figure 4b). The reduction potential for the negative part decreased by 50 mV, and that of the positive part increased by 70 mV, resulting in a 120 mV higher full cell voltage than alizarin (Figure 4c). Furthermore, we examined the high-potential cycled 2,3-CH_3-quinizarin electrode by ^{1}H NMR, confirming that most species are oxidized 2,3-CH_3-quinizarin (Figures S12 and S13). It is also possible to pair different quinones in an asymmetric setup. The (−) alizarin|1 M H_2SO_4|2,3-CH_3-quinizarin (+) showed a much-improved lifetime that retained 55% of its capacity after 500 cycles (Figure S14). Whereas the methylation of quinizarin increases the cycle life by blocking the Michael addition, the remaining sources of capacity fade are not clear at this early stage, in which the microstructure of the composite and the macrostructure of the cell and its operation have not been optimized. Varying the strength of adsorption by tailoring the chemical properties of the carbon or the quinone may change the rates of semiquinone production and decomposition. The current situation may be analogous to that of 2,6-dihydroxy-anthraquinone which decomposed at a rate of ∼5%/day when it was first introduced;[29] subsequent chemical modifications[21,23] and operating condition modifications[30] have reduced the fade rate by orders of magnitude.

In summary, we report a symmetric quinone-acid cell with 1.04 V of voltage and 163 mAh/g of specific capacity at 10C (see Table S1 for comparison with other aqueous batteries). The alizarin-based symmetric quinone-acid cell retains 45% of its capacity after 100 cycles with 100% of DoD. Our metal-free SQAB is potentially environmentally benign. The natural abundance and cheap commercial source promise its low cost when produced at large scale. We demonstrated with 2,3-dimethyl quinizarin that other fused quinone derivatives can also be used for symmetric quinone-acid batteries. The new chemistry and simple cell design provide a new platform for future optimization that can enable substantial cost reduction and rapid engineering development. Further optimization of fused quinones with improved reduction potential and stability, and cell engineering of electrode composition and morphology, can further improve the performance of the battery.

DOI: 10.1021/acsaem.9b00691
ACS Appl. Energy Mater. XXXX, XXX, XXX−XXX

■ ASSOCIATED CONTENT

Supporting Information

The Supporting Information is available free of charge on the ACS Publications website at DOI: 10.1021/acsaem.9b00691.

Materials and methods, synthesis of oxidized alizarin; electrochemistry of physisorbed alizarin, electrode material preparation, synthesis of quinizarin and derivatives and corresponding electrochemistry, and tabulated comparison of aqueous batteries (PDF)

■ AUTHOR INFORMATION

Corresponding Authors

*E-mail: gordon@chemistry.harvard.edu (R.G.G.).
*E-mail: maziz@harvard.edu (M.J.A.).

ORCID

Liuchuan Tong: 0000-0001-6211-6322
Yan Jing: 0000-0002-5669-4609
Roy G. Gordon: 0000-0001-5980-268X
Michael J. Aziz: 0000-0001-9657-9456

Author Contributions

§L.T. and Y.J. contributed equally.

Notes

The authors declare no competing financial interest.

■ ACKNOWLEDGMENTS

This work was partially funded through US Department of Energy ARPA-E Award DE-AR0000767, U.S. Department of Energy Contract DE-AC05-76RL01830 through PNNL Subcontract 428977, and the Massachusetts Clean Energy Technology Center. We thank Xian Gong for performing SEM imaging, Dr. Yunlong Ji for assistance with chemical synthesis, Dr. Qing Chen for assistance with electrochemical measurement, and Dr. Michael Marshak for helpful discussions.

■ REFERENCES

(1) Zubi, G.; Dufo-López, R.; Carvalho, M.; Pasaoglu, G. The lithium-ion battery: State of the art and future perspectives. *Renewable Sustainable Energy Rev.* **2018**, *89*, 292−308.

(2) Armand, M.; Tarascon, J. M. Building better batteries. *Nature* **2008**, *451*, 652.

(3) Few, S.; Schmidt, O.; Offer, G. J.; Brandon, N.; Nelson, J.; Gambhir, A. Prospective improvements in cost and cycle life of off-grid lithium-ion battery packs: An analysis informed by expert elicitations. *Energy Policy* **2018**, *114*, 578−590.

(4) Larcher, D.; Tarascon, J. M. Towards greener and more sustainable batteries for electrical energy storage. *Nat. Chem.* **2015**, *7* (1), 19−29.

(5) Beck, F.; Rüetschi, P. Rechargeable batteries with aqueous electrolytes. *Electrochim. Acta* **2000**, *45*, 2467.

(6) Chen, H. Y.; Li, A. J.; Finlow, D. E. The lead and lead-acid battery industries during 2002 and 2007 in China. *J. Power Sources* **2009**, *191* (1), 22−27.

(7) van der Kuijp, T.; Huang, L.; Cherry, C. R. Health hazards of China's lead-acid battery industry: a review of its market drivers, production processes, and health impacts. *Environmental Health* **2013**, *12* (61), 10.

(8) Zou, X.; Kang, Z.; Shu, D.; Liao, Y.; Gong, Y.; He, C.; Hao, J.; Zhong, Y. Effects of carbon additives on the performance of negative electrode of lead-carbon battery. *Electrochim. Acta* **2015**, *151*, 89−98.

(9) Rodrigues, L. E. O. C.; Mansur, M. B. Hydrometallurgical separation of rare earth elements, cobalt and nickel from spent nickel−metal−hydride batteries. *J. Power Sources* **2010**, *195* (11), 3735−3741.

(10) Kim, H.; Hong, J.; Park, K. Y.; Kim, H.; Kim, S. W.; Kang, K. Aqueous rechargeable Li and Na ion batteries. *Chem. Rev.* **2014**, *114* (23), 11788−827.

(11) Liang, Y.; Yao, Y. Positioning Organic Electrode Materials in the Battery Landscape. *Joule* **2018**, *2* (9), 1690−1706.

(12) Quan, M.; Sanchez, D.; Wasylkiw, M. F.; Smith, D. K. Voltammetry of Quinones in Unbuffered Aqueous Solution: Reassessing the Roles of Proton Transfer and Hydrogen Bonding in the Aqueous Electrochemistry of Quinones. *J. Am. Chem. Soc.* **2007**, *129*, 12847−12856.

(13) Jing, Y.; Liang, Y.; Gheytani, S.; Yao, Y. Cross-conjugated oligomeric quinones for high performance organic batteries. *Nano Energy* **2017**, *37*, 46−52.

(14) Huskinson, B.; Marshak, M. P.; Suh, C.; Er, S.; Gerhardt, M. R.; Galvin, C. J.; Chen, X.; Aspuru-Guzik, A.; Gordon, R. G.; Aziz, M. J. A metal-free organic-inorganic aqueous flow battery. *Nature* **2014**, *505* (7482), 195−8.

(15) Liang, Y.; Jing, Y.; Gheytani, S.; Lee, K.-Y.; Liu, P.; Facchetti, A.; Yao, Y. Universal quinone electrodes for long cycle life aqueous rechargeable batteries. *Nat. Mater.* **2017**, *16*, 841.

(16) Potash, R. A.; McKone, J. R.; Conte, S.; Abruña, H. D. On the benefits of a symmetric redox flow battery. *J. Electrochem. Soc.* **2016**, *163* (3), A338−A344.

(17) Suga, T.; Sugita, S.; Ohshiro, H.; Oyaizu, K.; Nishide, H. p- and n-Type bipolar redox-active radical polymer: Toward totally organic polymer-based rechargeable devices with variable configuration. *Adv. Mater.* **2011**, *23* (6), 751−4.

(18) Gao, H.; Goodenough, J. B. An aqueous symmetric sodium-ion battery with NASICON-structured $Na_3MnTi(PO_4)_3$. *Angew. Chem., Int. Ed.* **2016**, *55* (41), 12768−72.

(19) Suttil, J. A.; Kucharyson, J. F.; Escalante-Garcia, I. L.; Cabrera, P. J.; James, B. R.; Savinell, R. F.; Sanford, M. S.; Thompson, L. T. Metal acetylacetonate complexes for high energy density non-aqueous redox flow batteries. *J. Mater. Chem. A* **2015**, *3* (15), 7929−7938.

(20) Ma, T.; Pan, Z.; Miao, L.; Chen, C.; Han, M.; Shang, Z.; Chen, J. Porphyrin-based symmetric redox-flow batteries towards cold-climate energy storage. *Angew. Chem., Int. Ed.* **2018**, *57* (12), 3158−3162.

(21) Ji, Y.; Goulet, M.-A.; Pollack, D. A.; Kwabi, D. G.; Jin, S.; Porcellinis, D.; Kerr, E. F.; Gordon, R. G.; Aziz, M. J. A phosphonate-functionalized quinone redox flow battery at near-neutral pH with record capacity retention rate. *Adv. Energy Mater.* **2019**, *9*, 1900039.

(22) Gerhardt, M. R.; Tong, L.; Gómez-Bombarelli, R.; Chen, Q.; Marshak, M. P.; Galvin, C. J.; Aspuru-Guzik, A.; Gordon, R. G.; Aziz, M. J. Anthraquinone derivatives in aqueous flow batteries. *Adv. Energy Mater.* **2017**, *7*, 1601488.

(23) Kwabi, D. G.; Lin, K.; Ji, Y.; Kerr, E. F.; Goulet, M.-A.; De Porcellinis, D.; Tabor, D. P.; Pollack, D. A.; Aspuru-Guzik, A.; Gordon, R. G.; Aziz, M. J. Alkaline quinone flow battery with long lifetime at pH 12. *Joule* **2018**, *2*, 1907.

(24) Bien, H. S.; Stawitz, J.; Wunderlich, K. Anthraquinone Dyes and Intermediates. In *Ullmann's Encyclopedia of Industrial Chemistry*; Wiley-VCH, 2000.

(25) Carretero-González, J.; Castillo-Martínez, E.; Armand, M. Highly water-soluble three-redox state organic dyes as bifunctional analytes. *Energy Environ. Sci.* **2016**, *9*, 3521−3530.

(26) Yamamoto, N.; Kubozono, T.; Kinoshita, Y. Mechanism for oxidative decomposition of anthraquinone dye with hydrogen peroxide. *J. Oleo Sci.* **2001**, *50* (6), 507−513.

(27) Yang, B.; Hoober-Burkhardt, L.; Wang, F.; Surya Prakash, G. K.; Narayanan, S. R. An inexpensive aqueous flow battery for large-scale electrical energy storage based on water-soluble organic redox couples. *J. Electrochem. Soc.* **2014**, *161*, A1371−A1380.

(28) Tabor, D.; Gómez-Bombarelli, R.; Tong, L.; Gordon, R. G.; Aziz, M. J.; Aspuru-Guzik, A., Theoretical and experimental investigation of the stability limits of quinones in aqueous media: implications for organic aqueous redox flow batteries. *ChemRxiv* **2018** DOI: 10.26434/chemrxiv.6990053.v2.

DOI: 10.1021/acsaem.9b00691
ACS Appl. Energy Mater. XXXX, XXX, XXX−XXX

(29) Lin, K.; Chen, Q.; Gerhardt, M. R.; Tong, L.; Kim, S. B.; Eisenach, L.; Valle, A. W.; Hardee, D.; Gordon, R. G.; Aziz, M. J.; Marshak, M. P. Alkaline quinone flow battery. *Science* **2015**, *349* (6255), 1529.
(30) Goulet, M.-A.; Tong, L.; Pollack, D. A.; Tabor, D. P.; Odom, S. A.; Aspuru-Guzik, A.; Kwan, E. E.; Gordon, R. G.; Aziz, M. J. Extending the lifetime of organic flow batteries via redox state management. *J. Am. Chem. Soc.* **2019**, *141*, 8014.

NOTE ADDED AFTER ASAP PUBLICATION

Due to a production error, this paper was published on the Web on May 31, 2019, with errors in the first paragraph on page two of the document. The corrected version was reposted on June 4, 2019.

DOI: 10.1021/acsaem.9b00691
ACS Appl. Energy Mater. XXXX, XXX, XXX−XXX

Supporting Information

Symmetric All-Quinone Aqueous Battery

Liuchuan Tong,[▽,†] Yan Jing,[▽,†] Roy G. Gordon,[†,‡,] and Michael J. Aziz[†,*]*

[▽] Liuchuan Tong and Yan Jing contributed equally.

‡ Department of Chemistry and Chemical Biology, Harvard University, Cambridge, MA 02138, USA

‡ John A. Paulson School of Engineering and Applied Sciences, Harvard University, Cambridge, MA 02138, USA

* To whom correspondence should be addressed: gordon@chemistry.harvard.edu (Roy G. Gordon); maziz@harvard.edu (Michael J. Aziz).

Contents

Materials and Methods

Materials

All chemicals were purchased from Sigma Aldrich and used as received unless stated otherwise. Ketjenblack EC 600JD was obtained from Akzo Nobel Functional Chemicals, LLC. Spectracarb™

2225 Type 900 Activated Carbon Fabric was purchased from Engineered Fibers Technology, LLC. The separator, Celgard 3401, was obtained from Celgard Inc.

Chemical characterization and preparation

Proton nuclear magnetic resonance (^{1}H NMR) spectra were recorded using Varian INOVA 500 (500 MHz) NMR spectrometers at 23 °C. Proton chemical shifts are expressed in parts per million (ppm, δ scale) and are referenced to residual protium in the NMR solvent (DMSO-d_6, δ 2.50 ppm).

Synthesis of the oxidized alizarin

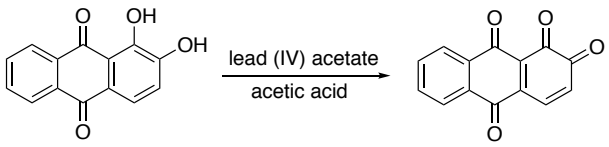

alizarin (480 mg, 2 mmol) was first suspended into 50 ml of diethyl ether, with vigorous stirring, lead dioxide (478 mg, 2 mmol) and 20 ml of acetic acid were then added to the suspension.[1] The reaction was stirred for 12 hours at room temperature. The final suspension was then filtrated to collect the greenish yellow cake, which was further dried under vacuum and used for characterization. Yield: 85%. ^{1}H NMR (500 MHz, DMSO-d_6): δ 8.04 – 7.98 (m, 1H), 7.96 – 7.91 (m, 1H), 7.85 (dd, J = 3.2 Hz, 2H), 7.47 (d, J = 16.3 Hz, 1H), 6.97 (d, J = 16.2 Hz, 1H).

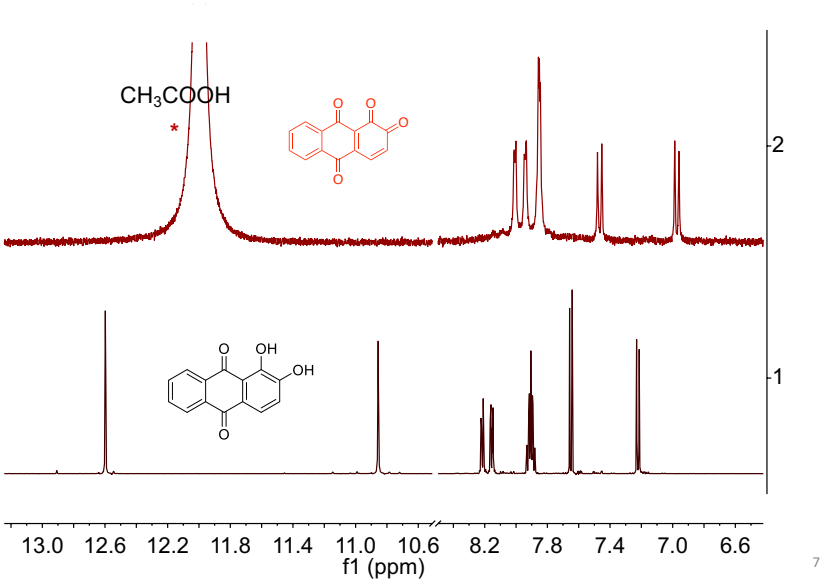

Figure S1. Highlighted aromatic regions of ^{1}H NMR spectra of pristine and oxidized alizarin in DMSO-D_6.

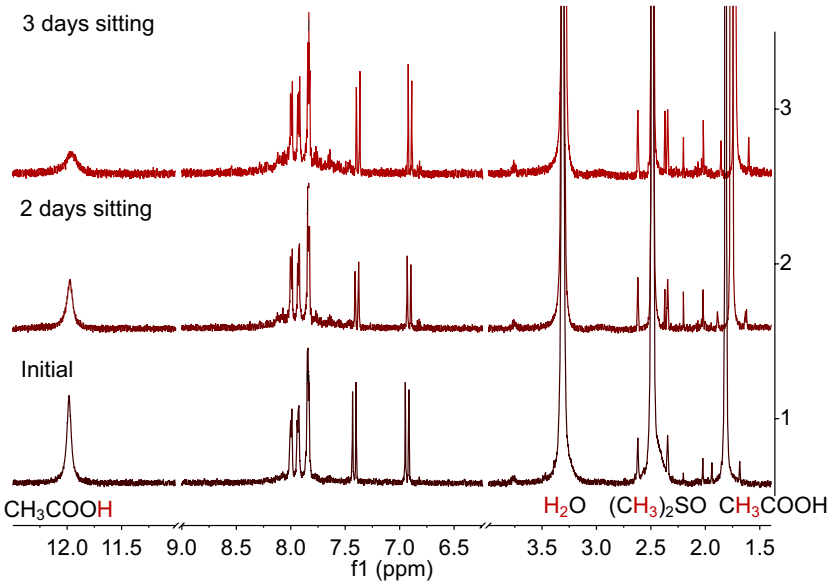

Figure S2. ^{1}H NMR spectra tracking of oxidized alizarin dissolved in DMSO-d_6 solvent with the presence of trace of acetic acid and water and kept for 2 days and 3 days, respectively. Most of the oxidized alizarin is still retained but some minor peaks appear in the aromatic region in the 3-day sitting sample, indicating slow decomposition. The NMR spectra in Figure S2 show the stability of oxidized alizarin in DMSO-d_6 with trace amount of acetic acid and water over three days.

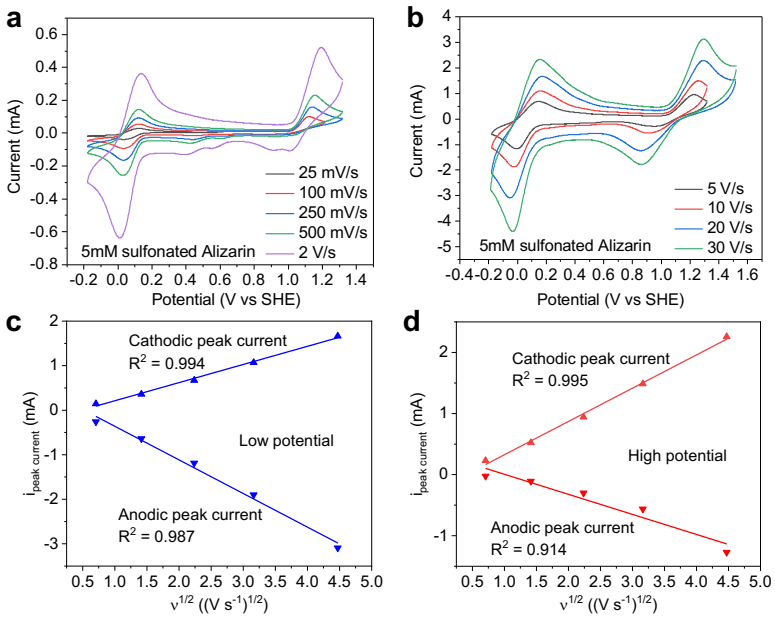

Figure S3. The cyclic voltammetry curves of 5 mM sulfonated alizarin in 1 M H_2SO_4 with varying scan rates (a, b): 0.025, 0.1, 0.25, 0.5, 2, 5, 10, 20, and 30 V/s. Sulfonated alizarin shows good electrochemical reversibility at low potential at any scan rate, but shows poor reversibility at high potential when the scan rate is less than 5 V/s. Good reversibility was obtained only when scanning faster than 5 V/s. (c): Cathodic and anodic peak current vs square root of scan rate (blue triangles) at low potential with linear fitting (blue lines). (d); Cathodic and anodic peak current vs square

root of scan rate (red triangles) at high potential with linear fitting (red lines). The selected scan rates are: 0.5, 2, 5, 10, and 20 V/s. The lowest R^2 value is given when linear fitting is performed for anodic peak current vs square root of scan rates at high potential, indicating the process is not completely diffusion-controlled.

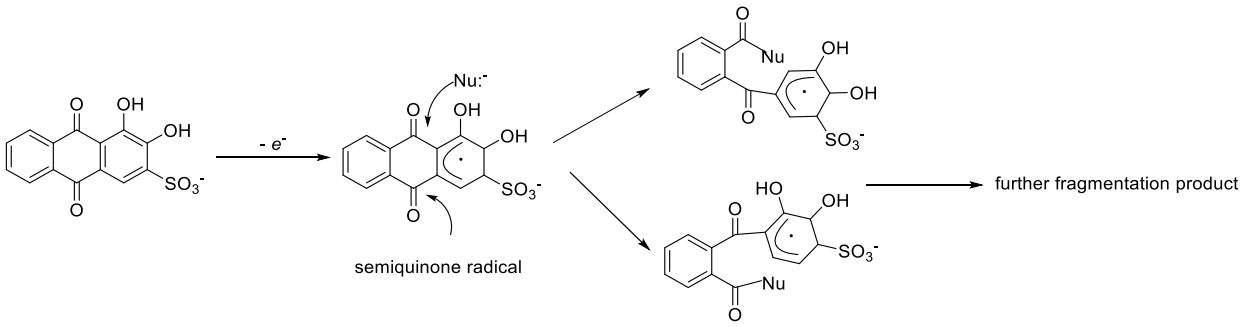

Scheme S1. The proposed decomposition pathways of sulfonated alizarin via electrochemical-chemical process.

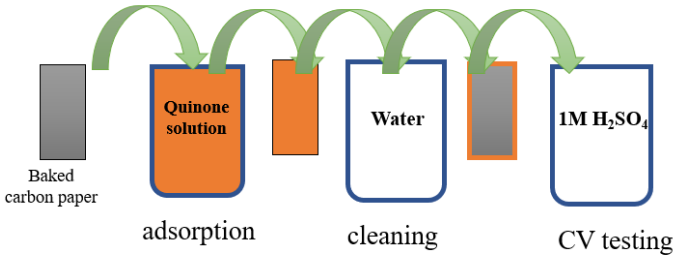

Scheme S2. Schematics of preparation for physisorption of alizarin on carbon paper.

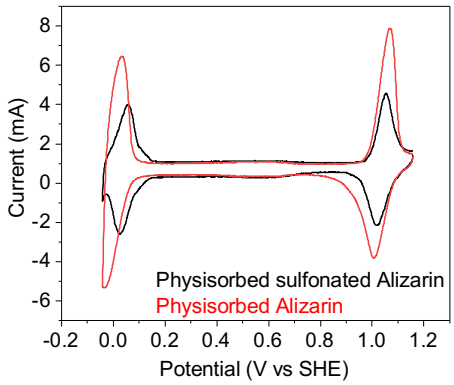

Figure S4. The CV curves of physisorbed alizarin and alizarin sulfonate in 1M H2SO4. When adsorbed to the carbon paper surface, both alizarin and sulfonated alizarin show good reversibility at both low and high potentials. San rate: 10 mV/s.

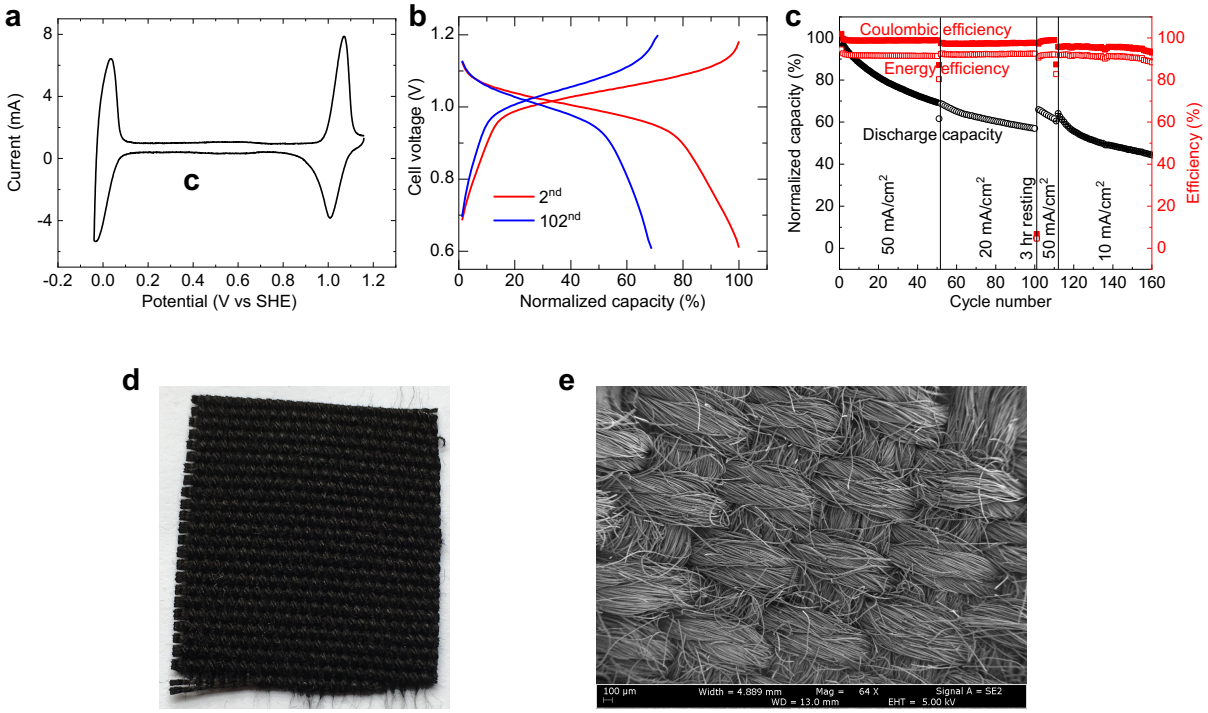

Figure S5. Electrochemical characterization of alizarin adsorbed on flexible Spectracarb™ 2225 carbon cloth (a) CV of alizarin adsorbed on carbon cloth. (b) Voltage profiles of adsorbed symmetric alizarin cell at 2nd and 102nd cycle, respectively. (c) Cycling performance of adsorbed symmetric alizarin pseudo-capacitor with varying current density. The cell was rested for 3 hours after 100th cycle. (d) Image of flexible Spectracarb™ 2225 carbon cloth. (e) SEM image of carbon cloth.

Electrode material preparation

Ball-milling and pellet preparation

Ball-milling was conducted at Harvard University Center for Nanoscale Systems on a Retsch PM 100 instrument. For a typical ball milling procedure, 0.6 grams of alizarin powder was mixed with 1.2 g of Ketjenblack and 0.2 g of graphite in a 125 mL grinding jar, and ball milled at 250 RPM for 2 hours with 10 × 4 g stainless steel ball, then at 500 RPM for 2 hours with 100 × 0.4 g stainless steel balls. The as-prepared alizarin: Ketjen black: graphite composite powder was then pressed by a hydraulic crimping machine to get pellets as the final electrode materials.

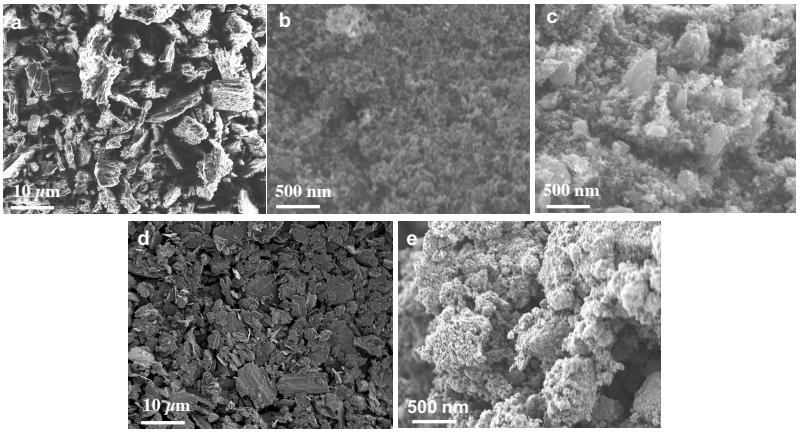

Figure S6. Scanning electron microscopy images. (a) As-received alizarin (b) As-received Ketjenblack (c) Ball-milled alizarin/Ketjenblack (d) Graphite (e) Ball-milled alizarin/Ketjenblack/graphite (w/w/w=3:6:1)

Electrolyte preparation

Concentrated sulfuric acid was diluted by deionized water to 1 M.

Electrochemical characterization

Carbon paper with/without physisorbed alizarin sulfonate as working electrode, an Ag/AgCl (3 M NaCl, 0.21 V *vs.* SHE) reference electrode, and a graphite rod as counter electrode were used for three-electrode cyclic voltammetry tests. In our home-made cell test, two graphite rods were used as both negative and positive current collectors, Ag/AgCl (1M KCl, 0.23 V *vs.* SHE) reference electrode was chosen as the reference electrode to fit our cell setup. All tests were carried out using a VMP3 Biologic Potentiostat and Galvanostat electrochemical workstation. For the 3-electrode cell setup, the potential of the working electrode is measured relative to the reference electrode. The working electrode was the capacity-limiting side, and the counter electrode was the non-capacity-limiting side with excess active material. When the oxidation of alizarin proceeds on the working electrode at high potential (~1 V vs SHE), the reduction of alizarin at low potential (0 V vs SHE) will presumably proceed on the counter electrode and vice versa.
The photos of home-made 3-electrode setup for cell performance evaluation. The graphite rods are used as current collectors, the Ag/AgCl (1M KCl, 0.23 V *vs.* SHE) is inserted right on top of the separator through a hole. There are two electrode pellets separated by a hydrophilic separator inside of the cell.

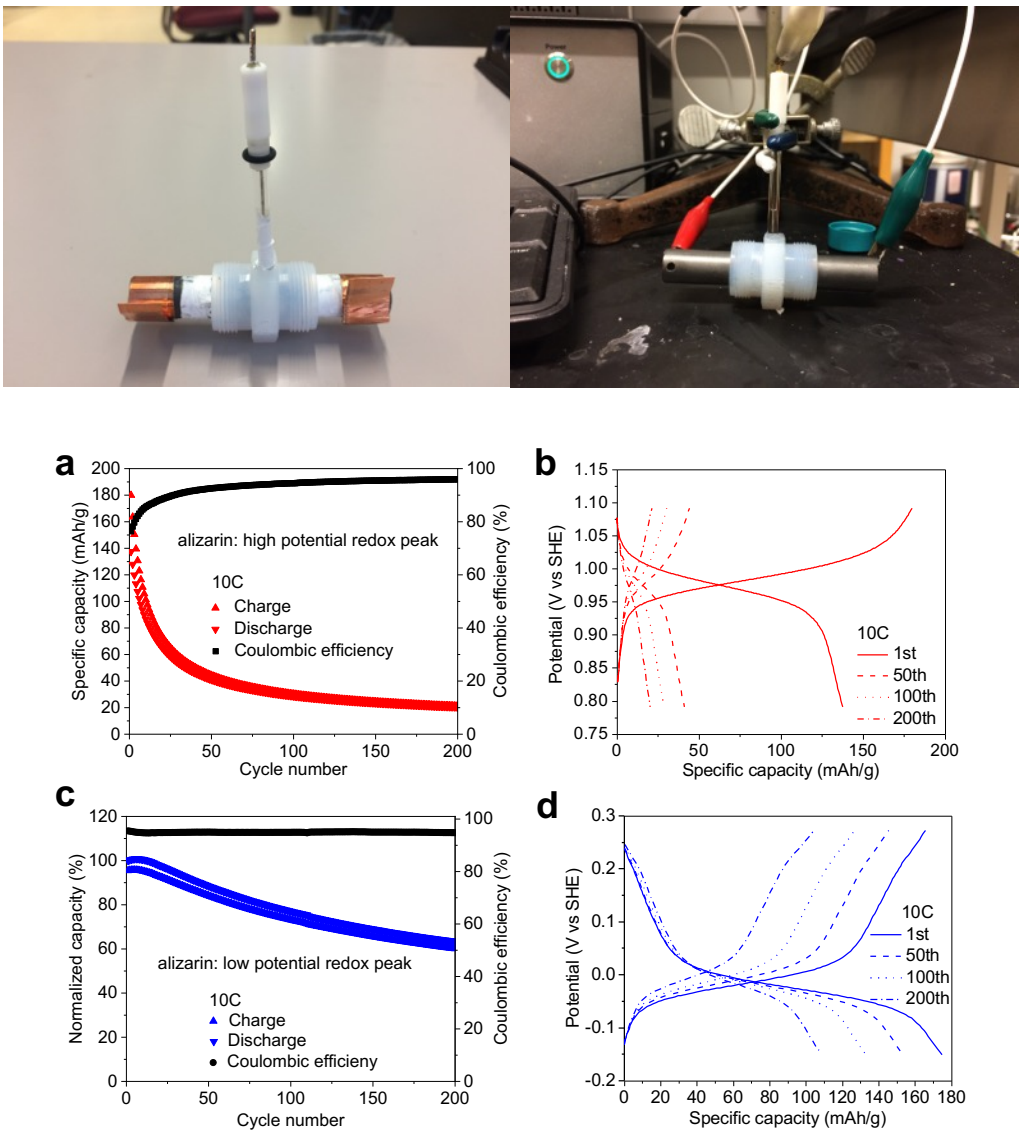

Figure S7. The cycle stability (a, c) and selected voltage profiles (b, d) of alizarin at both low (c, d) and high (a, b) potentials.

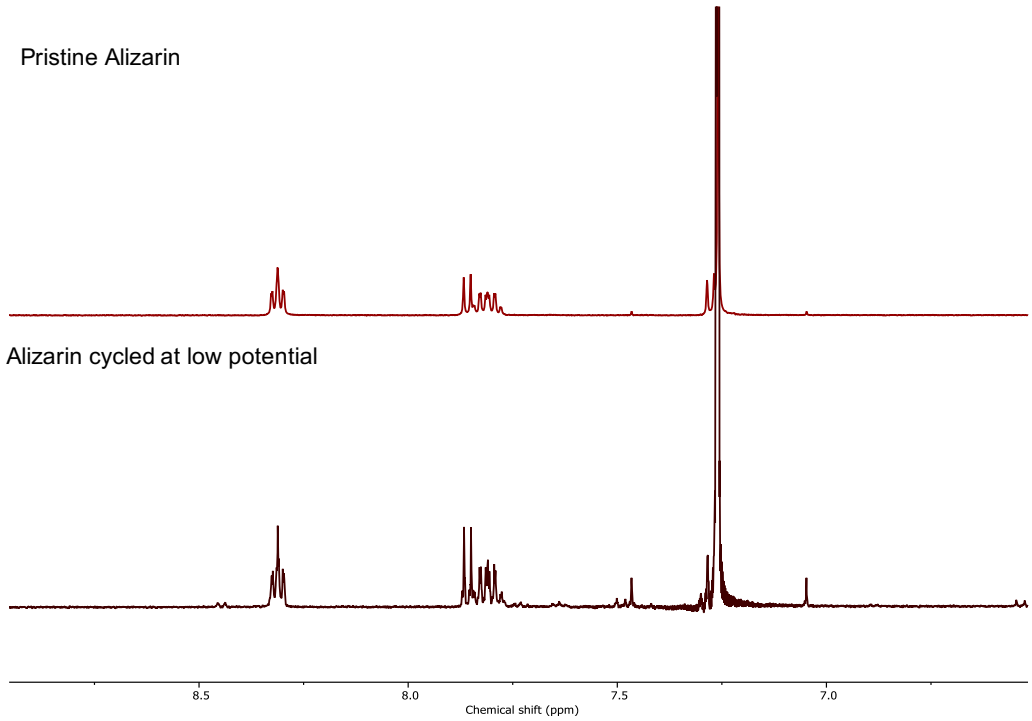

Figure S8. ^{1}H NMR spectra comparison of pristine and low-potential cycled alizarin in $CDCl_3$.

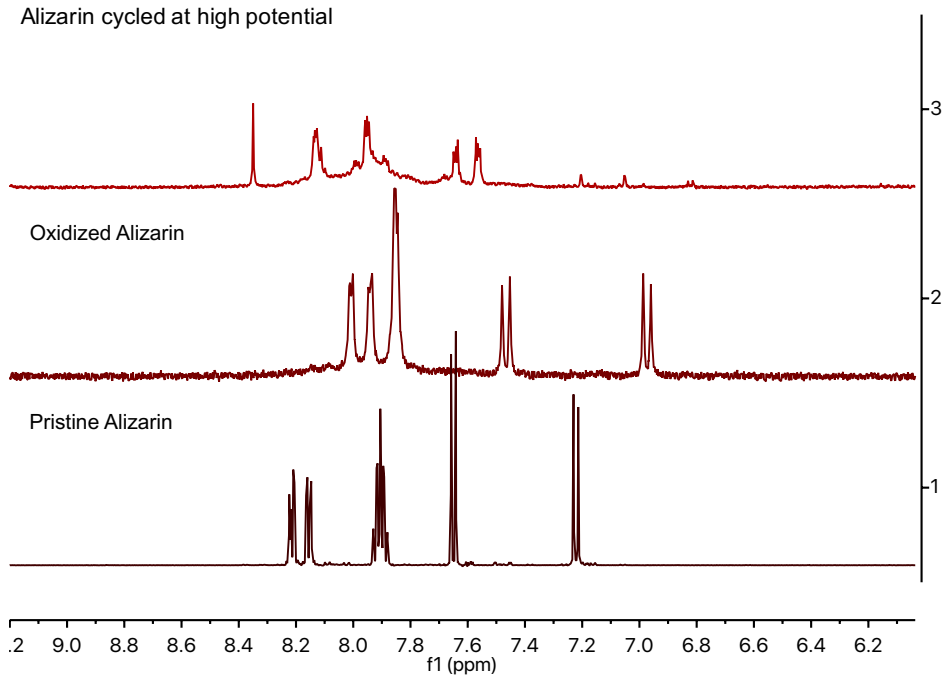

Figure S9. ^{1}H NMR spectra comparison of pristine (bottom), chemically oxidized (middle) and high-potential cycled alizarin (top). After cycling at high potential, some unknown peaks were observed in ^{1}H NMR, indicating the decomposition of alizarin. Solvent: DMSO-d_6.

Chemical oxidation of quinizarin

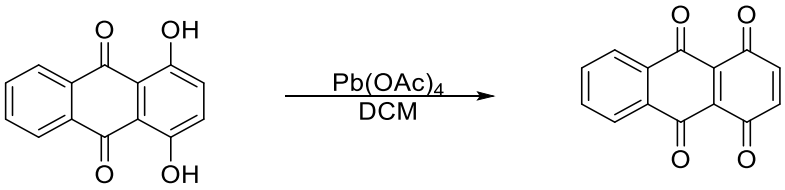

The synthesis of oxidized 2,3-dimethyl-quinizarin follows a literature report with modifications.[2] A mixture of quinizarin (1.00 g, 4.17 mmol) and lead tetraacetate (2.50 g, 5.64 mmol) in dichloromethane (100 mL) was stirred at room temperature for 6 h. The suspension was filtered and concentrated in vacuo. The brown solid was recrystallized from hot ethyl acetate (40 mL) to give a yellow powder. ^{1}H NMR (500 MHz, $CDCl_3$-d_6): δ 8.07 (dd, 2H), 7.83 (dd, 2H), 6.91 (s, 2H).

Synthesis of 2,3-dimethyl-quinizarin

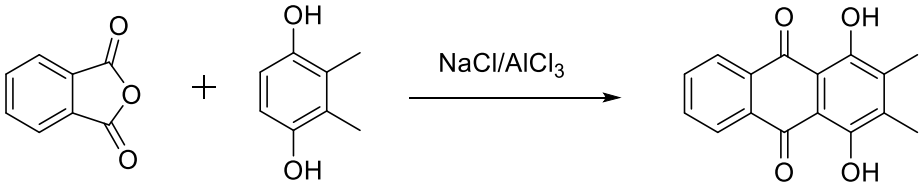

The synthesis of 2,3-dimethyl-quinizarin follows a literature report with modifications.[3]
A mixture of aluminum chloride (38 g) and sodium chloride (7.7 g) was melted in an Erlenmeyer flask at 180°C. To the melt was added an intimate mixture of phthalic anhydride (5.7g, 38.5 mmol) and 2,3-dimethylhydroquinone (5.2 g, 37.7 mmol). Red color immediately appeared and the reaction mixture was vigorously stirred at 180 ^{o}C for 5 min. The resulting red melt was cooled, ice water (200 mL) and hydrochloric acid (50 ml, 37%), were added, and the mixture was heated at 70 ^{o}C for 30 min. The resulting red precipitate was filtered, washed with water (100 mL) and dried to afford red powder (9.4 g, 93% yield). Additional acetic acid wash may be employed if impurities were observed by NMR. ^{1}H NMR (500 MHz, $CDCl_3$-d_6): δ 8.34 (dd, 2H), 7.80 (dd, 2H), 2.33 (s, 6H).

Chemical oxidation of 2,3-dimethyl-quinizarin

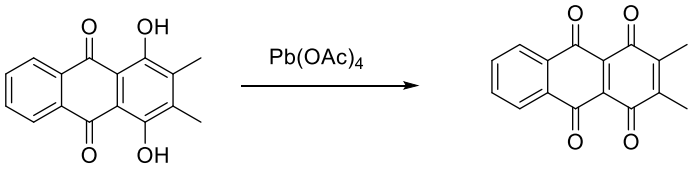

The synthesis of oxidized 2,3-dimethyl-quinizarin follows a literature report with modifications.[4]
A mixture of 2,3-dimethyl-quinizarin (500 mg, 1.8 mmol) and lead tetraacetate (1.8 g, 4.1 mmol) in toluene (200 mL) was refluxed at 100 ^{o}C for 6 h. After the reflux, the suspension was cooled to room temperature, filtered, and concentrated in vacuo. The brown solid was recrystallized from benzene to afford yellow powder (311 mg, 65% yield). ^{1}H NMR (500 MHz, $CDCl_3$-d_6): δ 8.06 (dd, 2H), 7.80 (dd, 2H), 2.10 (s, 6H).

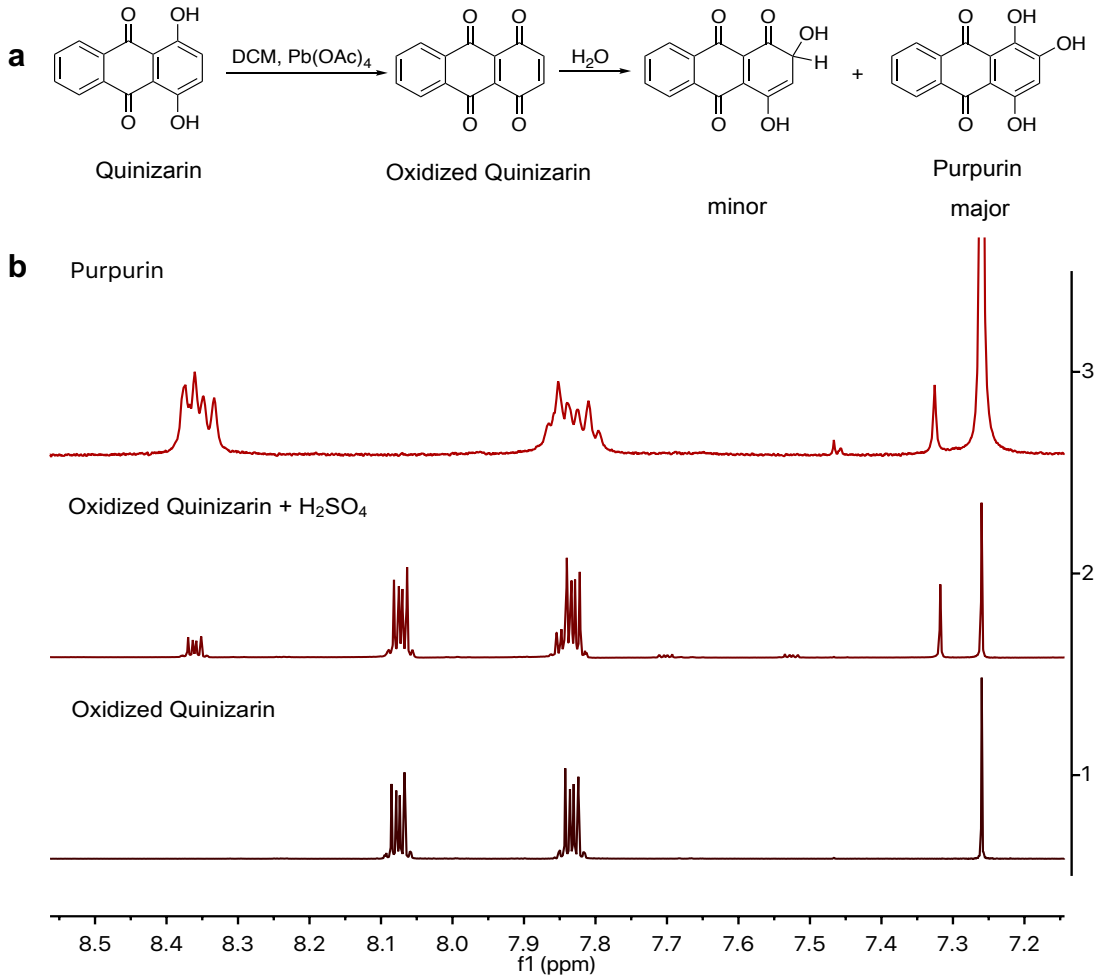

Figure S10. Demonstration that quinizarin in its oxidized form exhibits instability. (a) Scheme for the synthesis of oxidized quinizarin. (b) NMR spectra of pure oxidized quinizarin (top), oxidized quinizarin stirred with 1M H_2SO_4 solution for 12 hours (middle) showing additional peaks, pristine Purpurin (bottom). Solvent: $CDCl_3$. The NMR spectra in **Figure S10** show the instability of fully oxidized quinizarin when stirred with 1 M H_2SO_4 for 12 hours.

To prevent the Michael addition side reaction in fully oxidized fused quinones, we designed and fully oxidized 2,3-dimethyl-quinizarin to get its oxidized form, which shows improved stability over oxidized quinizarin in 1 M H_2SO_4 after 12 hours.

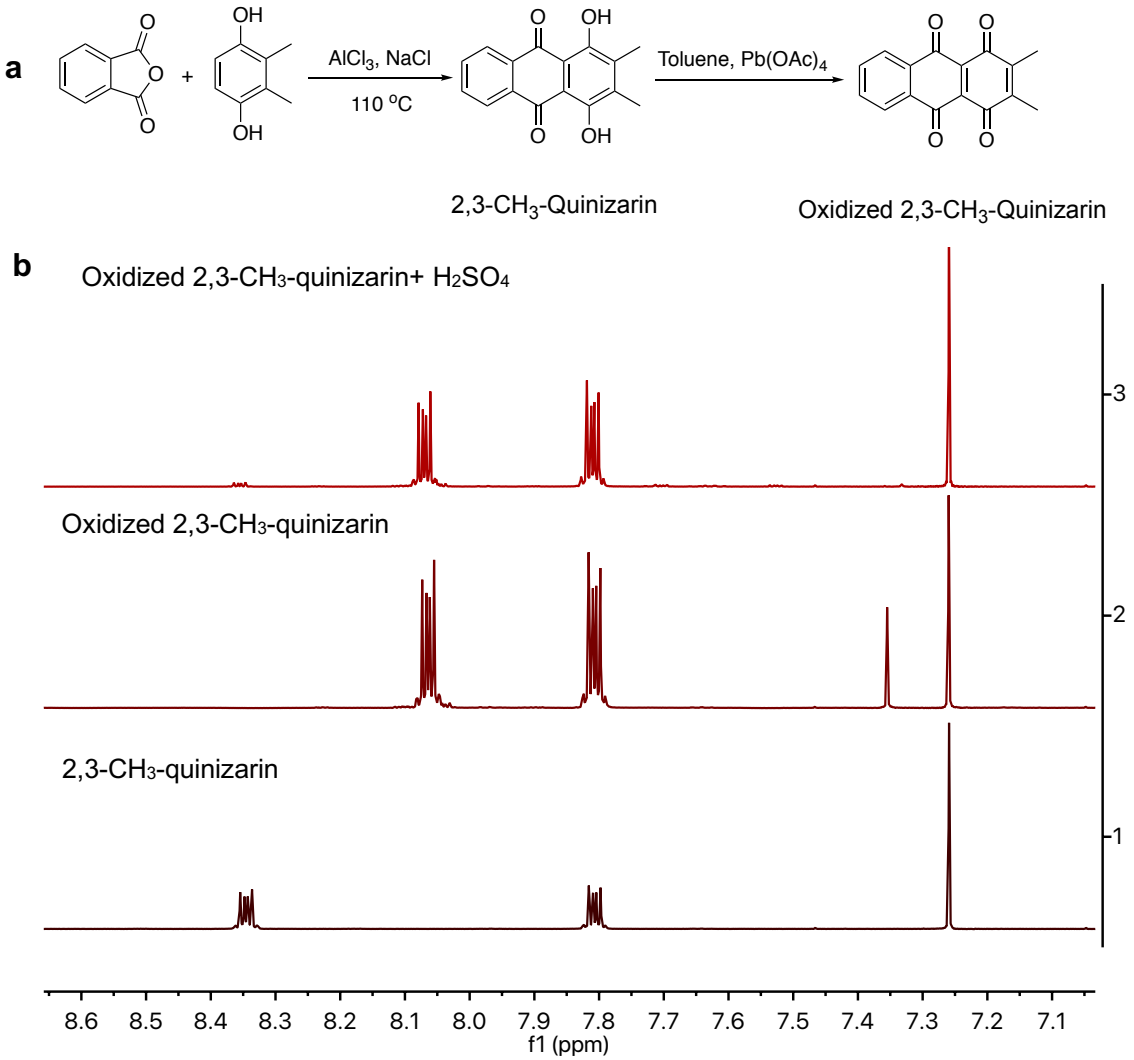

Figure S11. Demonstration that 2,3-dimethyl-quinizarin in its oxidized form exhibits improved stability over oxidized quinizarin. (a) Scheme for the synthesis of 2,3-dimethyl-quinizarin, and the synthesis of oxidized 2,3-dimethyl-quinizarin. (b) ^{1}H NMR spectra of pure 2,3-dimethyl-quinizarin (bottom), oxidized 2,3-dimethyl-quinizarin (middle) (the peak at 7.35 ppm is from an impurity that was subsequently washed away with water), and the oxidized 2,3-dimethyl-quinizarin stirred with 1 M sulfuric acid for 12 hours (top) showing a small peak at 8.3 ppm. No other decomposition was observed. Solvent: $CDCl_3$.

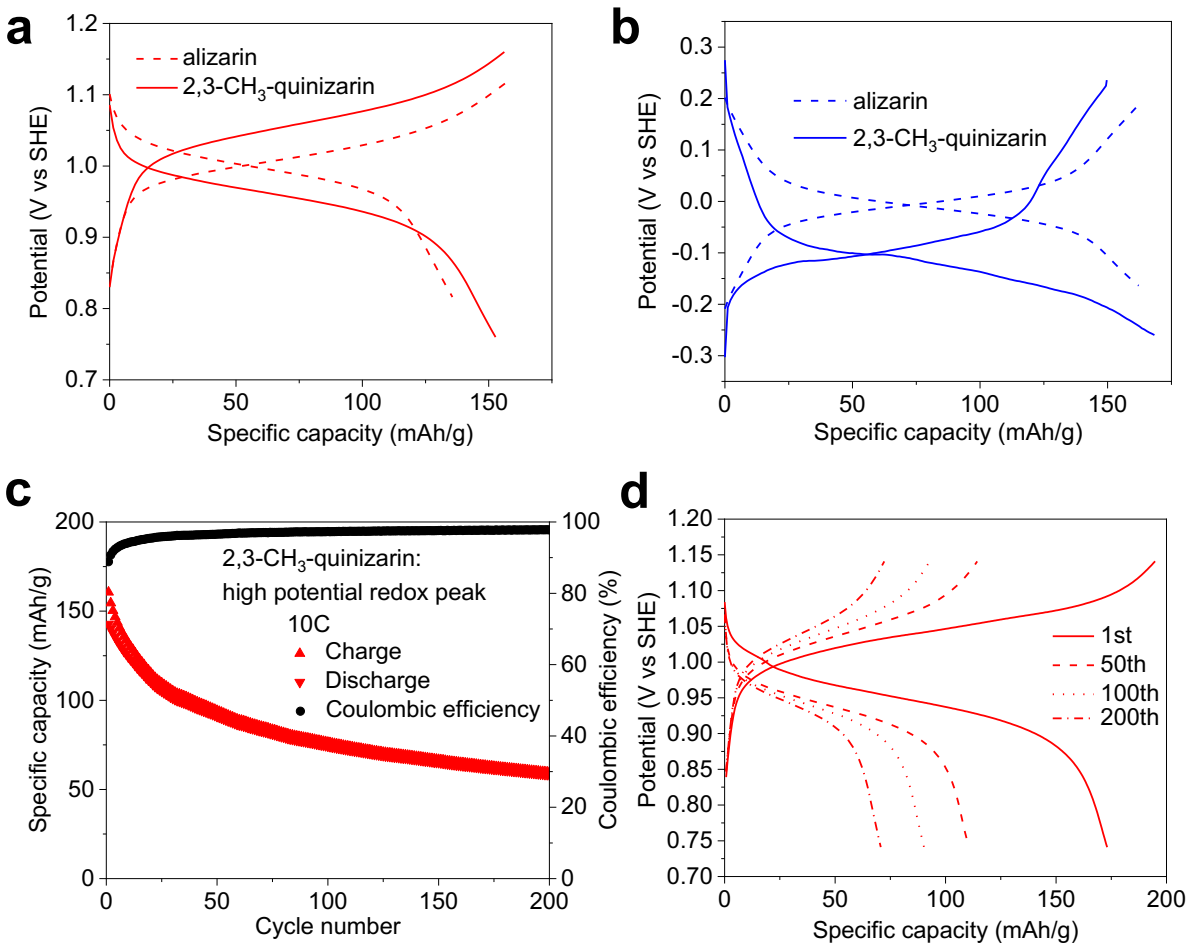

Figure S12. 2,3-dimethyl-quinizarin cell characterizations. (a, b) Voltage profiles of 2,3-dimethyl-quinizarin as cathode (a) and anode (b) materials compared to alizarin. (c, d) High-potential cycling and the selected voltage profile of 2,3-dimethyl-quinizarin.

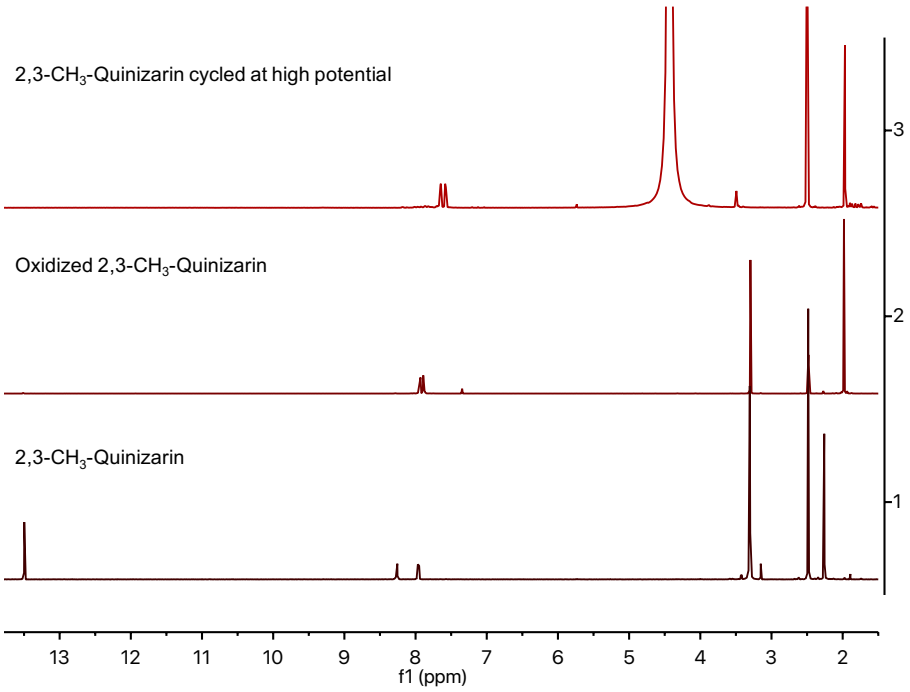

Figure S13. ^{1}H NMR spectra of pristine (bottom), chemically oxidized (middle) and cathode-cycled (top) 2,3-dimethyl-quinizarin. Solvent: DMSO-d_6.

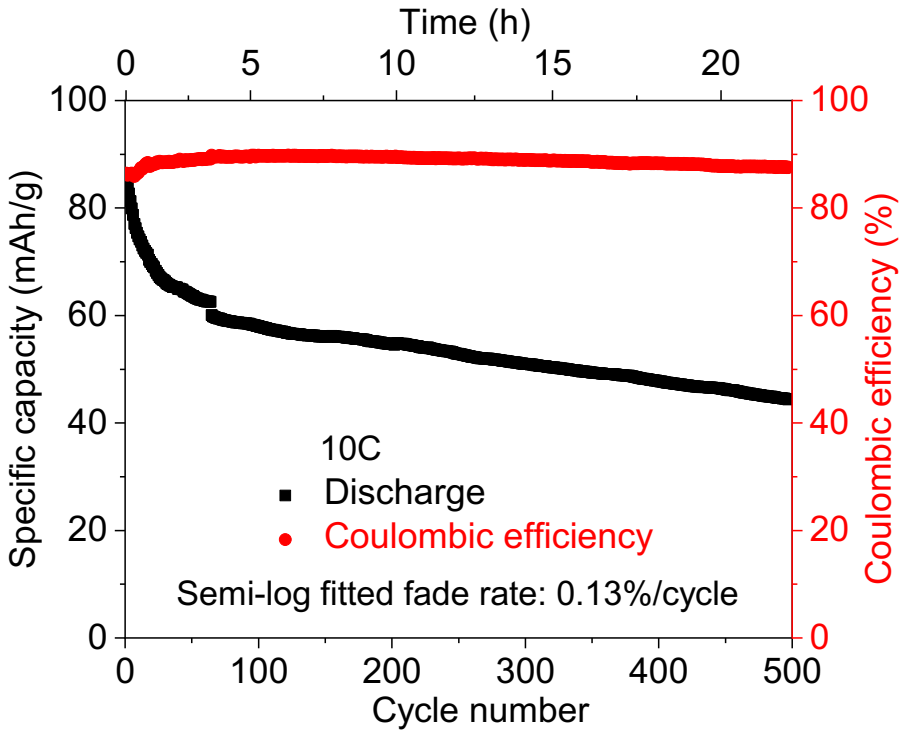

Figure S14. Cycling of the cell (–) alizarin | 1 M H_2SO_4 | 2,3-dimethyl-quinizarin (+). The specific capacity is based on the total quantity of active materials on both electrodes.

Table S1. The composition and electrochemical characteristics of representative aqueous secondary batteries.

Electrolyte / pH		Charge carriers	Anode / potential (V vs SHE) / Specific capacity (mAh/g)			Cathode / potential (V vs SHE) / Specific capacity (mAh/g)			Volt. (V)	Theoretical specific energy at 100% DoD (Wh/kg)	Ref.
H_2SO_4	–1	H^+, HSO_4^-	Pb	-0.34	258	PbO_2	1.76	159	2.05	171	[5]
H_2SO_4	-1	H^+, HSO_4^-	PTO	0.51	409	$PbSO_4$	1.76	159	1.25	114	[6]
H_2SO_4	-1	H^+, HSO_4^-	AC	0.48	50*	PbO_2	1.76	159	1.28	49	[7-8]
H_2SO_4	**0**	**H^+**	**alizarin**	**0.01**	**223**	**alizarin**	**1.05**	**223**	**1.04**	**116**	**This work**
Li_2SO_4	7	Li^+	$LiTi_2(PO_4)_3$	-0.50	138	$LiFePO_4$	0.50	170	1.00	76	[9]
Na_2SO_4	7	Na^+	PPTO	-0.07	229	$Na_3V_2(PO_4)_3$	0.65	117	0.72	56	[6]
Na_2SO_4	7	Na^+	$Na_3MnTi(PO_4)_3$	-0.59	59	$Na_3MnTi(PO_4)_3$	0.81	59	1.40	41	[10]
KOH	15	H^+	MmH	-0.81	300	NiO(OH)	0.39	292	1.20	177	[11]

PTO: pyrene-4,5,9,10-tetraone; AC: activated carbon; PPTO: polymerized PTO; MmH: metal hydride; *: the specific capacity (electric double layer) of activated carbon is an experimental value. Specific capacity (mAh/g) is calculated by F × n / MW / 3.6. F: Faraday constant (96485 C/mol); n: number of electrons transferred during reaction; MW: molecular weight of organic compound or molar mass of inorganic compound (g/mol). Theoretical specific energy (Wh/kg) is calculated by (F × n / total MW / 3.6) × U. Total MW: the sum of molecular weight/molar mass from all participated species in a reaction. For $Pb/PbO_2/PbSO_4$-based chemistries, we considered the contribution from electrolyte (H_2SO_4) for all calculations.

Table S1 describes eight representative aqueous batteries with different electrode materials and chemistries. For those acidic batteries involving Pb, sulfuric acid participates in redox reactions on electrodes; therefore, the mass of electrolyte should be included in reckoning the specific capacity. In the symmetric AQAB, in contrast, the electrolyte does not participate in the redox reactions the amount of electrolyte can be minimized. Many other aqueous batteries utilize toxic or expensive metals such as vanadium, cadmium, cobalt, and etc. The symmetric AQAB is completely metal-free, environmentally friendly, and potentially cost effective. In addition, the smallest charge carrier (proton) in the SQAB makes the smallest changes in both volume and mass of redox-active material, potentially leading to the lowest mechanical stress of electrodes. The two-electron transfer process endows alizarin a theoretical specific capacity of 223 mAh/g, which is comparable to that of most inorganic electrode materials.

Supplementary References

1. Gorelik, M. V., Synthesis and properties of 1,2,9,10-anthracenetetrone. *Journal of Organic Chemistry of the USSR* **1968,** (4), 501−506.
2. J. Bingham, S.; H. P. Tyman, J., The synthesis of kermesic acid and isokermesic acid derivatives and of related dihydroxyanthraquinones. *J. Chem. Soc., Perkin Trans. 1* **1997,** (24), 3637−3642.

3. Kerdesky, F. A. J.; Cava, M. P., A novel synthesis of (.+-.)-4-demethoxydaunomycinone. *Journal of the American Chemical Society* **1978,** *100* (11), 3635–3636.
4. Kerdesky, F. A. J.; Ardecky, R. J.; Lakshmikantham, M. V.; Cava, M. P., Simple o-quinodimethane route to (.+-.)-4-demethoxydaunomycinone. *Journal of the American Chemical Society* **1981,** *103* (8), 1992–1996.
5. Ruetschi, P., Aging mechanisms and service life of lead–acid batteries. *Journal of Power Sources* **2004,** *127* (1–2), 33–44.
6. Liang, Y., Jing, Y., Gheytani, S., Lee, K-Y., Liu, P., Facchetti, A., Yao, Y., Universal quinone electrodes for long cycle life aqueous rechargeable batteries. *Nat. Mater.* **2017,** *16*, 8.
7. Zou, X., Kang, Z., Shu, D., Liao, Y., Gong, Y., He, C., Hao, J., Zhong, Y., Effects of carbon additives on the performance of negative electrode of lead-carbon battery. *Electrochimica Acta* **2015,** *151*, 89–98.
8. Yu, N.; Gao, L.; Zhao, S.; Wang, Z., Electrodeposited PbO_2 thin film as positive electrode in PbO_2/AC hybrid capacitor. *Electrochimica Acta* **2009,** *54* (14), 3835–3841.
9. Luo, J. Y.; Cui, W. J.; He, P.; Xia, Y. Y., Raising the cycling stability of aqueous lithium-ion batteries by eliminating oxygen in the electrolyte. *Nat. Chem.* **2010,** *2* (9), 760–765.
10. Gao, H.; Goodenough, J. B., An aqueous symmetric sodium-ion battery with NASICON-structured $Na_3MnTi(PO_4)_3$. *Angew. Chem. Int. Ed.* **2016,** *55* (41), 12768–12772.
11. Ovshinsky, S. R.; Fetcenko, M. A.; Ross, J., A nickel metal hydride battery for electric vehicles. *Science* **1993,** *260*, 176–181.